Thermally Induced Polytype Transformations among the Layered Double Hydroxides (LDHs) of Mg and Zn with Al

Grace S. Thomas,[†] A. V. Radha,[†] P. Vishnu Kamath,*[,†] and S. Kannan*[,‡]

Department of Chemistry, Central College, Bangalore University, Bangalore 560 001, India, and Silicates and Catalysis Discipline, Central Salt and Marine Chemicals Research Institute, G.B. Marg, Bhavnagar 364 002, India

Received: March 6, 2006; In Final Form: April 29, 2006

The hydrotalcite-like layered double hydroxide (LDH) of Mg with Al shows dramatic changes in the peaks arising from the (*h*0*l*)/(0*kl*) family of reflections in its powder X-ray diffraction pattern during thermal treatment. DIFFaX simulations show that these changes arise due to the transformation of the disordered $3R_1$ polytype into the 1H polytype on dehydration. The 1H polytype is an essential precursor to the decomposition reaction, which results in the formation of an oxide residue with the rock salt structure. In contrast, the LDH of Zn with Al does not undergo any such transformation, retaining the structure of the $3R_1$ polytype until decomposition into the oxide residue. Given the poor octahedral site preference of the Zn^{2+} ion, the 1H polytype is neither structurally stable nor is it topochemically necessary for the thermal decomposition of the Zn−Al LDH, the end product of the decomposition reaction being an oxide with the wurtzite structure.

Introduction

Many divalent hydroxides $M(OH)_2$ (M = Mg, Fe, Co, Ni, Cd) crystallize in the structure of mineral brucite, $Mg(OH)_2$.[1] Brucite comprises a hexagonal close packing of hydroxyl ions with cations occupying alternate layers of octahedral sites. This results in a stacking of charge-neutral layers having the composition $[Mg(OH)_2]$. If upper case symbols A, B, and C represent the hydroxyl ion positions, and lower case symbols a, b, and c represent the cation positions, then the stacking sequence in brucite is AbC AbC ... Such a stacking sequence is given the symbol 1H, with 1 representing the single layered periodicity and H standing for the hexagonal structure.[2] In such a structure, if a fraction *x* of the divalent metal ions is replaced by a trivalent ion M′(III) [M′(III) = Al, Cr, Fe, Ga], the brucite slabs, AbC, acquire a positive charge which is compensated by anions accommodated within the interlayer. The resultant compound is called a layered double hydroxide (LDH) and can be represented by the general formula $[M(II)_{1-x}M'(III)_x(OH)_2](A^{n-})_{x/n}\cdot yH_2O$ (A = CO_3^{2-}, NO_3^-, Cl^-).[3] The layer stacking sequence in LDHs can be represented as AbCX AbCX ... where X represents the anion position. In this illustrative sequence, X corresponds to the octahedral B sites. If, however, the anion in question has a preference for other sites, it would mediate the stacking of the metal hydroxide sheets into other sequences, giving rise to new polytypes. Carbonates are known to prefer trigonal prismatic sites, whereas the sulfates are found to occupy both trigonal prismatic and octahedral sites.[4] A prismatic interlayer site is generated when the lower hydroxyls of a brucite-like slab occupy the same sites as the upper hydroxyls of the slab below. Bookin and Drits[2] have examined by both experiment and theory the complete range of polytypes possible among the LDHs. Some of the common polytypes are the following:

AC CB BA AC... $3R_1$

AC BA CB AC... $3R_2$

AC CA AC CA... $2H_1$

AC AB CB AC... $3H_2$

In this nomenclature, the cation positions and interlayer sites are not specified, being self-evident. Naturally occurring CO_3^{2-}-containing LDHs are known to crystallize in the $3R_1$ and $2H_1$ polytypes. The mineral forms of the $3R_1$ and $2H_1$ polytypes of the Mg−Al LDH, $Mg_6Al_2(OH)_{16}CO_3\cdot 4H_2O$, are known as hydrotalcite and manasseite, respectively.[3] SO_4^{2-}-containing LDHs exhibit greater polytype diversity and crystallize in the $3R_1$, $3R_2$, $3H_2$, and 1H polytypes.[4] A schematic polyhedral representation illustrating the stacking sequences of the 1H, $2H_1$, and $3R_1$ polytypes is shown in Figure 1. The structures of the other polytypes can be similarly visualized.

Aside from their anion exchange properties,[6] the LDHs are widely used as precursors for the low-temperature synthesis of oxide catalysts.[7] Consequently, the thermal decomposition of the hydrotalcite-like Mg−Al−CO_3^{2-} LDH has been widely studied by numerous authors using different in situ as well as ex situ techniques. These include variable-temperature powder diffraction,[7,8] TGA and isothermal heating,[9] MAS NMR,[10] and evolved gas analysis (EGA).[11] These citations are representative rather than being comprehensive, and a more complete review of the thermal behavior of the LDHs can be found elsewhere.[12] From these studies, there is a general understanding that HT undergoes a two-step mass loss on heating. The low-temperature (100−250 °C) step corresponds to the loss of interlayer water (dehydration) while the high-temperature (∼450 °C) step corresponds to decomposition. Decomposition involves the

* To whom correspondence should be addressed. E-mail: vishnukamath8@hotmail.com (P.V.K.), skannan@csmcri.org (S.K.).
† Bangalore University.
‡ Central Salt and Marine Chemicals Research Institute.

10.1021/jp061377f CCC: $33.50
Published on Web 06/08/2006

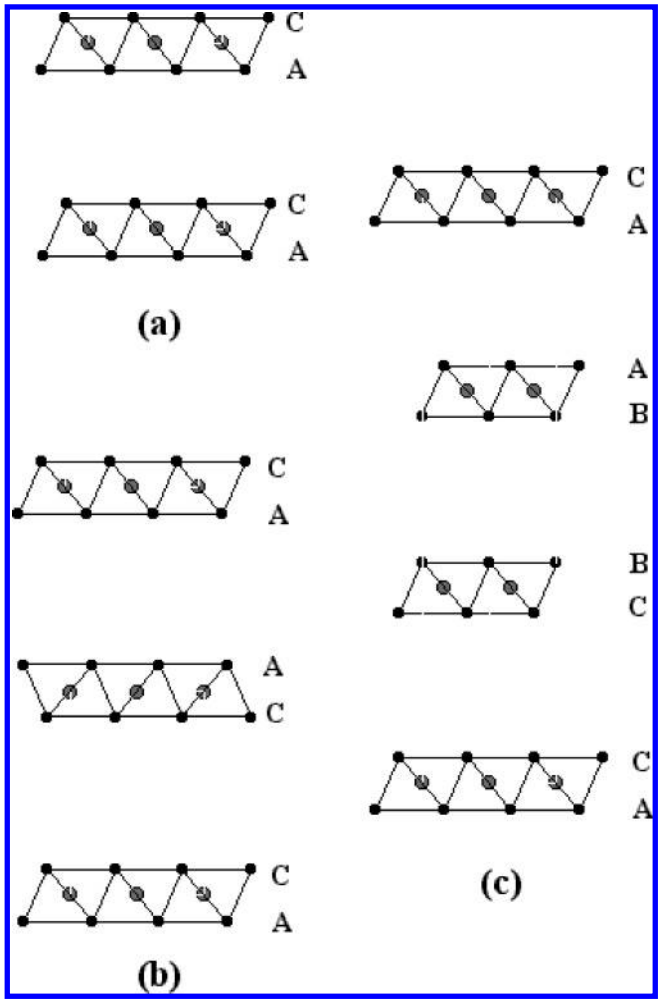

Figure 1. Schematic polyhedral representation of the structures of the (a) 1H, (b) $2H_1$, and (c) $3R_1$ polytypes showing the corresponding stacking sequences. Interlayer anions are not shown for purpose of clarity.

simultaneous deanation (loss of intercalated CO_3^{2-}) and dehydroxylation of the layers.

Within the HT structure, the oxygen atoms of intercalated CO_3^{2-} as well as H_2O occupy a single set of crystallographic sites.[13] It was our surmise that, during the topotactic dehydration of the LDH, the decrease in the occupancy of interlayer sites ought to profoundly affect the stacking of metal hydroxide slabs. This could arise not only from the forces of friction and drag involved in the removal of water molecules from the confined spaces in the interlayer region of the LDH but also from packing considerations as octahedral interlayer sites provide a more efficient packing compared to prismatic interlayer sites. The latter facilitate hydrogen bonding between the hydroxyl ions of the slabs and the intercalated species, and when hydrogen bonding depletes on account of dehydration, prismatic sites are expected to lose thermodynamic stability. Structural changes observed during LDH calcination have been studied by several authors with a focus on (1) the bonding and symmetry of the CO_3^{2-} anion[14] and (2) the evolution of oxide phases.[15] In this work, we examine how different polytypes evolve on calcination of the CO_3^{2-} containing Mg−Al and Zn−Al LDHs.

Experimental Methods

Hydrotalcite was synthesized by the method of Reichle[16] by the slow addition of a mixed metal ($Mg^{2+} + Al^{3+}$) nitrate solution (total concentration 1.2 M) containing Mg^{2+} and Al^{3+} in the ratio 2:1 to a solution containing the stoichiometric requirement of OH^- ions and three times the stoichiometric requirement of CO_3^{2-} taken as Na_2CO_3. The precipitation was carried out at 25 °C. The resultant precipitate was aged in the mother liquor at 90 °C for 24 h before being filtered, washed, and dried to constant weight. The Zn−Al−CO_3^{2-} LDH was prepared by the addition of a mixed-metal ($Zn^{2+} + Al^{3+}$) nitrate solution (100 mL) containing the stoichiometric ratio of the two metal ions to 100 mL of a Na_2CO_3 solution containing three times the stoichiometric requirement of carbonate ions. The pH of the mixture was maintained at 10 by the simultaneous addition of 1.0 M NaOH solution using a Metrohm model 718 Stat Titrino. The precipitation was carried out at 60 °C, and then the precipitate was aged in the mother liquor at 60 °C for 72 h before being filtered, washed, and dried to constant weight.

In situ variable-temperature powder X-ray diffraction (VT-PXRD) was carried out on a Philips X'pert MPD system connected to an Anton-Paar high-temperature XRK assembly using Cu Kα radiation. The sample was mounted in a high-temperature cell and heated at 5 °C min^{-1} in steps of 25 °C and stabilized for 10 min before measurements. The operating voltage and current were 40 kV and 4 mA, respectively. The step size was 0.05° with step time of 1 s.

Thermogravimetric studies were carried out in a Mettler Toledo TGA/SDTA 851^e, Star^e 7.01 system from 30 to 750 °C (heating rate 5 °C min^{-1}, flowing air).

DIFFaX Simulations. The PXRD patterns of the LDHs were simulated using the Fortran-based code DIFFaX.[17] Within the DIFFaX formalism,[18] a crystalline solid is treated as a stacking of layers of atoms interconnected by stacking vectors: an approach that is ideally suited for layered materials. Details of the DIFFaX simulations of the PXRD patterns of LDHs are given elsewhere[19,20] and summarized here.

The metal hydroxide layer, AC, was defined using the atomic position coordinates of HT taken from the literature (ICSD no. 6296). For the Zn−Al−CO_3^{2-} LDH, the position coordinates were obtained by doing a Rietveld refinement of the structure using the profile recorded at ambient temperature (space group $R\bar{3}m$, $a = 3.071$ Å, $c = 22.729$ Å) (data not shown).

The Bragg reflections of different polytypes were computed by stacking the layers one above another with different stacking vectors. To facilitate comparison with experimental data, the calculated Bragg peaks were broadened using a Lorentzian line shape. The fwhm of the 110 peak was selected for the Lorentzian line-width as this reflection is relatively unaffected by stacking disorders. The width of the 110 peak for the ambient temperature PXRD patterns of both LDH systems was found to be 0.3° in 2θ. As DIFFaX is not a profile refinement program, the use of a Lorentzian profile function is found to be adequate to simulate the line broadening and has been successfully used in earlier papers.[19−20] The instrumental line width determined for the Si standard over 77−28° 2θ was found to be 0.2−0.15° in 2θ.

To simulate a pure $3R_1$ polytype, we define an AC layer and use the stacking vector ($^2/_3$, $^1/_3$, $^1/_3$). The use of the stacking vector (0, 0, 1) on the other hand yields the 1H polytype. To simulate the $2H_1$ polytype we define two layers AC and CA and stack them using the vector (0, 0, $^1/_2$). If we use more than one stacking vector, with different probabilities, the random intergrowth of more than one polytype is simulated. Other stacking vectors simulate structural disorder. For instance, turbostraticity can be simulated using the stacking vector (x, y, 1) where x and y are random. On the introduction of structural disorder, the peaks in the PXRD pattern are nonuniformly

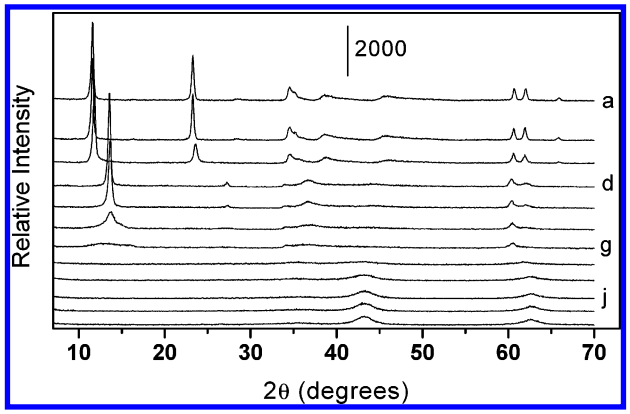

Figure 2. In situ variable-temperature PXRD patterns of the Mg−Al LDH calcined in air at different temperatures (°C): (a) 50, (b) 150, (c) 200, (d) 250, (e) 275, (f) 300, (g) 325, (h) 375, (i) 425, (j) 500, (k) 550, (l) 600.

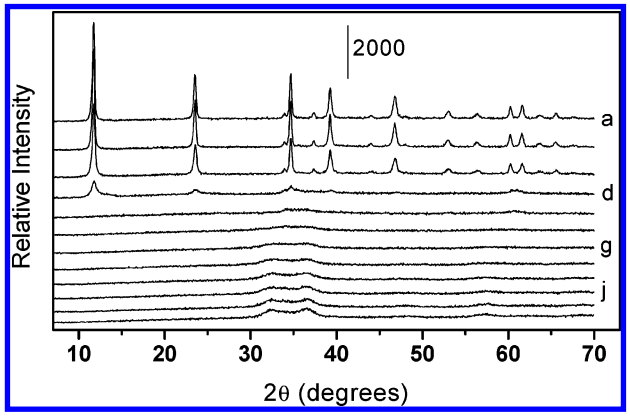

Figure 3. In situ variable-temperature PXRD patterns of the Zn−Al LDH calcined in air at different temperatures (°C): (a) 50, (b) 100, (c) 150, (d) 175, (e) 225, (f) 275, (g) 350, (h) 400, (i) 450, (j) 500, (k) 550, (l) 600.

broadened and the DIFFaX code computes the resultant diffraction profile. The probabilities of the use of different stacking vectors are varied until a good fit between the calculated and observed patterns is obtained. The goodness-of-fit is determined by the matching of peak positions and fwhm values to within ±0.1° in 2θ and the relative intensities within ±5%. The probabilities then correspond to the percentage incidence of the corresponding polytype/disorder. Crystallite size effects can also be simulated by varying the disc diameter measured along the *ab*-plane and the thickness of the crystallites measured along the crystallographic *c*-axis.

Results and Discussion

Figures 2 and 3 show the in situ VTPXRD patterns of the CO_3^{2-} containing Mg−Al and Zn−Al LDHs, respectively. The PXRD patterns recorded at the ambient temperature agree with those reported earlier for these systems.[21,22] The PXRD pattern of an LDH has the following three distinct regions: (1) There is the low angle region (5−25° 2θ) containing the basal reflections (00*l*). This is characteristic of the size of the interlayer anion. For carbonate-containing LDHs, these appear at 11.6° 2θ (7.6 Å) and 23.3° 2θ (3.8 Å), respectively. (2) Also, there is the high angle region (50−65 °2θ) containing the (*hk*0) and (*hkl*) reflections. These are characteristic of the metal hydroxide layer. Since the metal hydroxide layer remains invariant, the high angle regions remain the same for all polytypes. (3) The mid-2θ region (30−50°2θ) contains the (*h*0*l*)/(0*kl*) reflections. Different polytypes can be distinguished from one another by

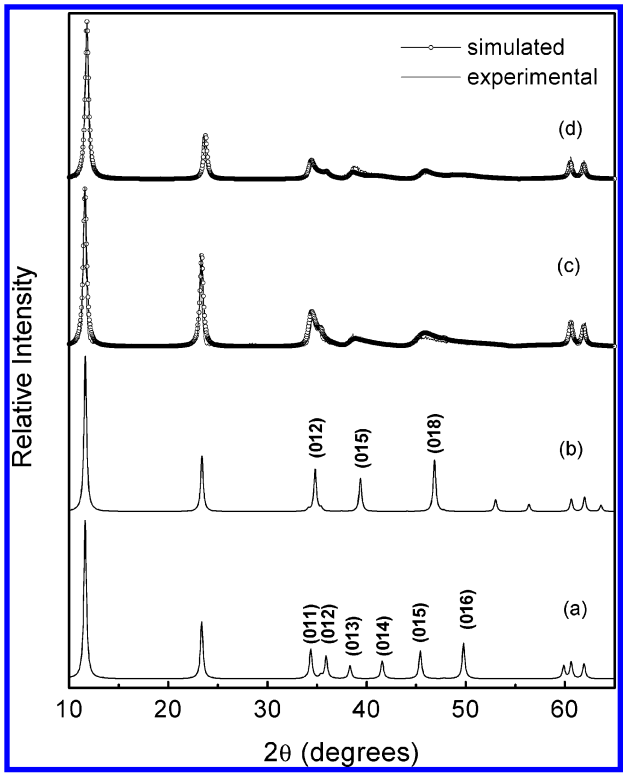

Figure 4. DIFFaX simulated PXRD patterns of the model (a) $2H_1$ and (b) $3R_1$ polytypes. A comparison of the experimental patterns of the Mg−Al LDH obtained at (c) ambient temperature and (d) 200 °C with the corresponding DIFFaX simulations is also shown.

the reflections appearing in the mid-2θ region.[19,23] Turbostratic disorder as well as random intergrowths of different polytypes affect this region.[24]

Among the carbonate containing LDHs, the polytypes of interest are the $3R_1$ and $2H_1$ as both offer trigonal prismatic interlayer sites. Figure 4a,b shows the DIFFaX simulated patterns of model structures belonging to the $3R_1$ and $2H_1$ polytypes, respectively. In Figure 4c is shown the observed pattern of the Mg−Al LDH. The peak positions in the mid-2θ region match with those expected for the $3R_1$ polytype, but the nonuniform broadening of lines was simulated by the random intergrowth of the $3R_1$ and $2H_1$ polytypes in equal proportions, in agreement with previous results.[20,25]

On heating, the following changes are observed in the PXRD patterns of Mg−Al LDH: (1) There is a progressive decrease in the relative intensity of the (002*l*) reflection with respect to the (00*l*) up to 200 °C. (2) In the temperature range 250−300 °C, the (00*l*) reflection shifts to a higher 2θ value (13.6° 2θ, 6.5 Å). Together with this, there are changes in the number and line shapes of the reflections appearing in the mid-2θ region. (3) Above 375 °C, features corresponding to the oxide residue begin to emerge. Similar observations have been made by Vaysse and co-workers[14] in the Ni−Fe and Ni−Co LDHs.

As explained elsewhere,[19] the atoms in the interlayer diffract out of phase with the metal hydroxide slabs. Consequently, the relative intensities of the (00*l*) and (002*l*) reflections depend on the electron density in the interlayer region. During dehydration (100−250 °C), this decreases rapidly resulting in a sharp increase in the intensity of the (00*l*) relative to the (002*l*) reflection. The PXRD pattern in Figure 2c was simulated by decreasing the interlayer O from 1.25 to 0.9 (see Figure 4d). The relative intensity of the (002*l*) reflection observed in Figure 2d could be simulated using a fully dehydrated LDH corresponding to 0.5 O in the interlayer. The latter corresponds only

TABLE 1: Summary of the DIFFaX Simulations

$Mg_{0.67}Al_{0.33}(OH)_2(CO_3)_x \cdot yH_2O$, 0.4 Lorentzian

			crystallite size (Å)		
T (°C)	polytype mix	interlayer water (*y*)	disc diameter (Å)	layer thickness (Å)	CO_3^{2-} content (*x*)
50	50% $3R_1$ + 50% $2H_1$	0.75	∞	∞	0.166
200	40% $3R_1$ + 60% $2H_1$	0.39	∞	∞	0.166
250	40% turbostratic 1H	0	∞	∞	0.125
300	50% turbostratic 1H	0	∞	65.2	0.120

$Zn_{0.67}Al_{0.33}(OH)_2(CO_3)_{0.165} \cdot yH_2O$

			crystallite size (Å)		
T (°C)	polytype	interlayer water	disk diameter (Å)	layer thickness (Å)	Lorentzian
50	$3R_1$	1.0	∞	∞	0.3
150	$3R_1$	0.82	∞	378	0.3
175	80% turbostratic$3R_1$	0.5	1000	303	0.2

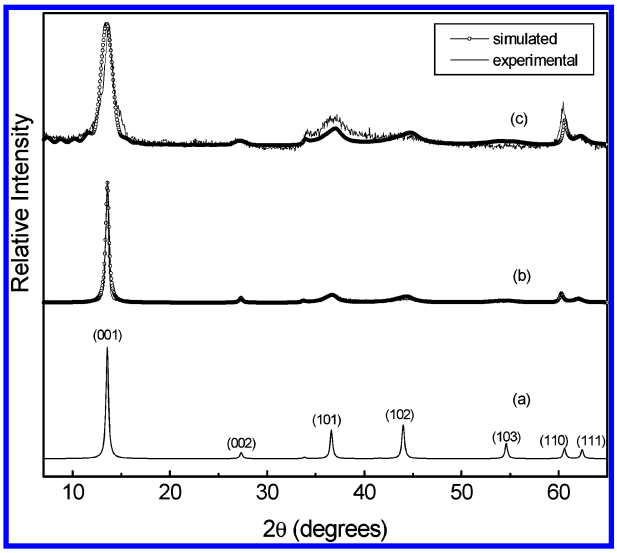

Figure 5. (a) DIFFaX simulated PXRD pattern of the 1H polytype. (b) Part a with 40% turbostratic disorder compared with the experimental pattern of Mg−Al LDH obtained at 250 °C. (c) DIFFaX simulated PXRD pattern of the disordered 1H polytype including crystallite size effects compared with the experimental pattern of Mg−Al LDH obtained at 300 °C.

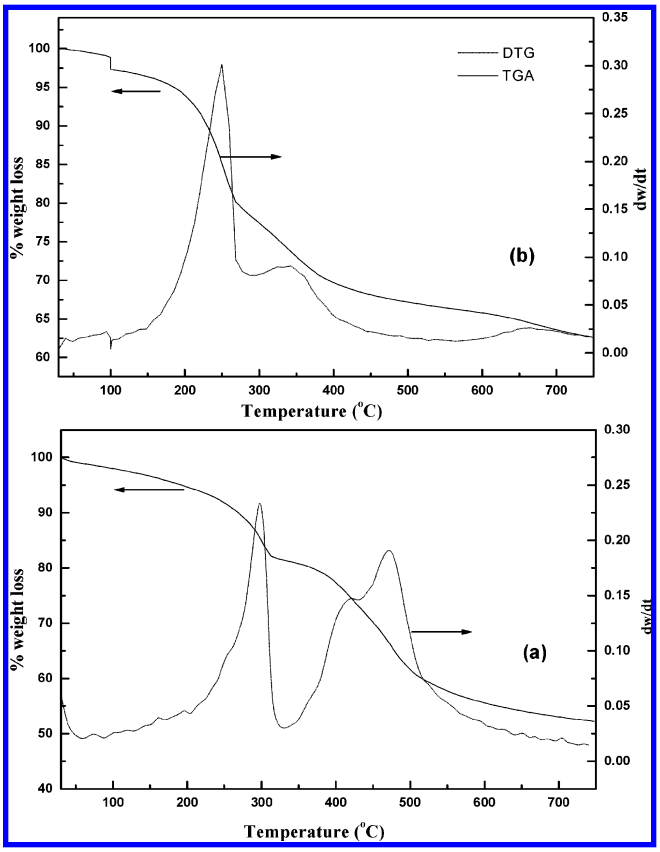

Figure 6. TGA and DTG data of the as-prepared (a) Mg−Al and (b) Zn−Al LDHs.

to the carbonate content. The complete loss of water understandably results in a decrease in the interlayer spacing from 7.6 to 6.5 Å.

The PXRD pattern in Figure 2d shows other changes in the mid-2θ region indicating a possible change in the polytype upon dehydration. Figure 5a shows the DIFFaX simulated PXRD pattern expected of the 1H polytype. Though the mid-2θ reflections in the observed pattern at Figure 2d are very broad, their peak positions match well with those calculated for the 1H polytype. The line broadening points to the incidence of structural disorder. The final DIFFaX solution was obtained by introducing 40% of turbostratic disorder into the 1H polytype (Figure 5b). These simulations indicate the transformation of the disordered $3R_1$ polytype to the 1H variety on dehydration. During this transformation, the width of the low-angle reflection (00*l*) remains unchanged. This is to be expected as stacking faults and turbostratic disorder do not affect the line shape of the basal reflections.[26]

The PXRD pattern of the LDH at 300 °C (Figure 2f) shows a broadening of the basal reflections as well. This was simulated by introducing particle size effects into the solution shown in Figure 5b (see Figure 5c). The reduction in particle size is expected in the context of the loss of interlayer matter upon dehydration. Indeed, the loss of nearly 18% (computed from TG data, Figure 6) of the solid mass as volatile matter is expected to cause the break up of the crystallites of the original hydroxide leading to the formation of a nanoparticulate residue.[27] DIFFaX simulations indicate a particle size of 6.5 nm corresponding to a stacking of 10 layers.

Bellotto et al.[28] have published the PXRD pattern of a dehydrated Mg−Al LDH which matches with what we report in Figure 2f. They attribute the decrease in the basal spacing upon heating to the migration of Al^{3+} ions from octahedral sites within the metal hydroxide slabs to tetrahedral sites in the interlayer. However, the DIFFaX simulation based on this structure model not only fails to generate the 006 reflection but also does not predict the peak positions of the reflections appearing in the mid-2θ region (see Figure 11 of ref 28). The simulations reported here in Figure 5 based on a turbostratically disordered 1H structure are superior.

Table 1 summarizes the results of the simulations.

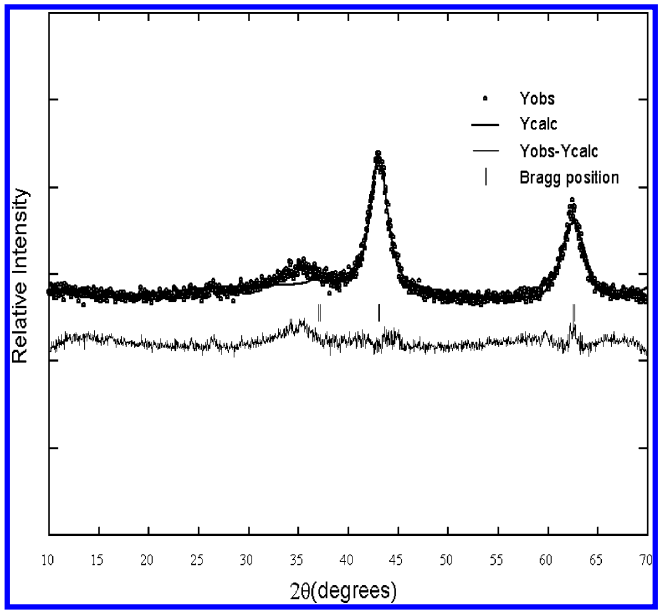

Figure 7. Rietveld refinement of the structure of the defect periclase using the PXRD profile of the oxide residue obtained from the Mg−Al LDH at 600 °C.

Above 375 °C, the oxide residue gradually evolves and transforms to a poorly ordered oxide phase (Figure 2h,i). We show by Rietveld refinement (Figure 7) that the oxide residue at 600 °C is a defect rock salt phase with 33% Al replacing Mg in the MgO structure resulting in the composition $Mg_{0.572}Al_{0.285}\square_{0.143}O$. Periclase MgO (ICSD no. 95468) was used as the starting model, and a 12 coefficient polynomial was used to fit the background. A total of 20 parameters were refined to fit the pattern. Though the goodness-of-fit parameters (R_p = 39.6, R_{wp} = 21.7, R_{Bragg} = 4.2, R_F = 5.9) are not within the acceptable range, considering the poor crystallinity of the residue, the fit can be regarded as satisfactory. The formation of an oxide with the defect rock salt structure has been suggested earlier.[29] Indeed, the poor stability of the defect rock salt oxide is responsible for the reversible thermal behavior of HT.[9−10,27]

The changes in the PXRD pattern of the Mg−Al LDH can also be related to its TGA data (see Figure 6a). Mg−Al LDH shows a two step mass loss, while the DTG shows three points of inflection. The highest temperature feature (472 °C) in the DTG corresponds to the high-temperature tail (500−750 °C) in the TGA which is due to the slow release of gas from the micropores of the oxide residue on sintering.[30] As sintering continues to temperatures well above 1000 °C, the tail in the TG extends to high temperatures. This feature is universally present in all LDHs including the Zn−Al LDH (Figure 6b) where it starts at ∼325 °C itself.

The Mg−Al LDH progressively loses mass at T > 100 °C, and at 275 °C the dehydration is complete according to the following reaction (observed mass loss = 17.8%; expected mass loss = 16.4%):

$$Mg_{0.67}Al_{0.33}(OH)_2(CO_3)_{0.163}\cdot 0.75H_2O \rightarrow Mg_{0.67}Al_{0.33}(OH)_2(CO_3)_{0.163}$$

The phase obtained at this temperature is characterized by the PXRD pattern at Figure 2d corresponding to the 1H polytype. The second point of inflection appears at 422 °C. At this temperature, the PXRD pattern (Figure 2i) shows features due to the oxide residue. The following reaction corresponds to the decomposition reaction (observed mass loss = 30.0%; expected mass loss = 36.6%):

$$Mg_{0.67}Al_{0.33}(OH)_2(CO_3)_{0.163} \rightarrow Mg_{0.67}Al_{0.33}O_{1+0.163} + H_2O + 0.163CO_2$$

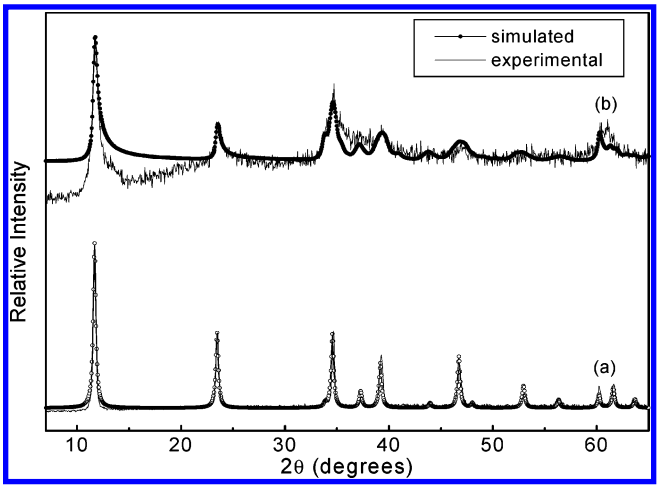

Figure 8. DIFFaX simulated PXRD patterns of the Zn−Al LDH compared with the patterns observed at (a) ambient temperature and (b) 175 °C.

The Zn−Al LDH crystallizes in the structure of an ordered $3R_1$ polytype (Figure 8a). The positions of the peaks in the mid-2θ region of the PXRD pattern of the Zn−Al LDH remains unchanged up to 175 °C, showing that there is no change in the polytype during heat treatment (Figure 3). The major change is the gradual reduction in the relative intensity of the (006) reflection relative to the (003), for reasons already explained above. Figure 8b shows the experimental and simulated PXRD patterns of the Zn−Al LDH at 175 °C. The asymmetric broadening of lines in the mid-2θ region is indicative of stacking disorder while the decrease in the intensities of the 00l reflections suggests particle size effects.[24] The final solution was obtained by the introduction of turbostratic disorder (80%) in the $3R_1$ polytype. Broadening of the basal reflection was simulated by including particle size effects (thickness = 30.3 nm, 40 layers). The intensity of the 006 reflection relative to 003 was simulated by decreasing the intercalated water content to $0.5H_2O$ (see Table 1). Above this temperature, there is a collapse of the layered structure as evidenced by the complete extinction of the basal reflections (Figure 3e). Features corresponding to the oxide residue appear at 225 °C. We show by means of a Rietveld refinement (Figure 9) that this oxide residue is a defect wurtzite ZnO wherein 33% of the Zn^{2+} sites are occupied by the Al^{3+} ions. The structural model used for the refinement was wurtzite ZnO (ICSD no. 44058). A 6 coefficient polynomial was used to fit the background and a Pearson VII function to fit the line shape. A total of 20 parameters were refined. The following goodness of fit parameters were obtained: R_p = 38.5, R_{wp} = 24.5, R_{Bragg} = 8.5, R_F = 5.7. The absence of a polytype transformation prior to decomposition is supported by TGA data (see Figure 6b) which shows a single step mass loss at 250 °C. At this temperature, the LDH structure has completely broken down (see Figure 3e).

The thermodynamic and structural factors governing the stability of polytypes among LDHs have been described elsewhere.[20] As the metal hydroxide slab and the interlayer remain invariant across different polytypes, hydrogen bonding is the chief determinant of polytype selectivity. Extensive hydrogen bonding exists between OH^- ions of the slabs and

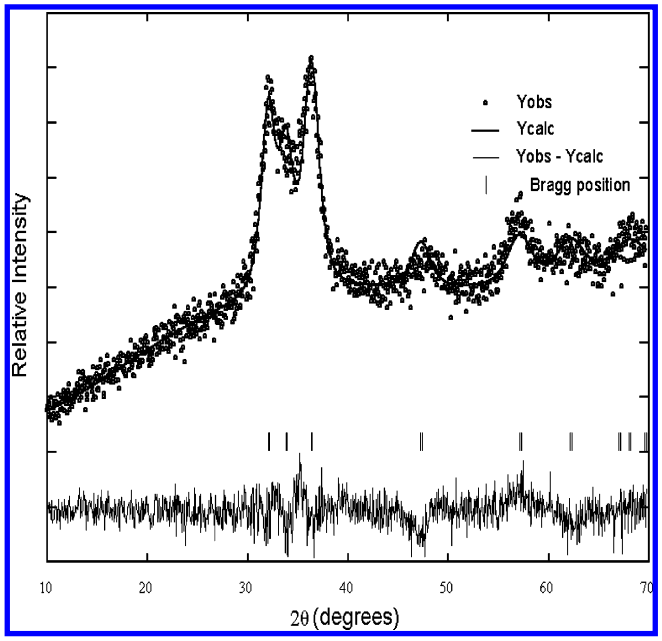

Figure 9. Rietveld refinement of the structure of defect wurtzite using the PXRD profile of the oxide residue obtained from the Zn−Al LDH at 600 °C.

the intercalated species. For the CO_3^{2-} anion in D_{3h} symmetry, hydrogen bonding with the metal hydroxide slab is maximized in prismatic sites. This explains why the naturally occurring Mg−Al−CO_3^{2-} LDH crystallizes only in the $3R_1$ and $2H_1$ polytypes. Synthetic Mg−Al LDH such as the one used here is disordered and contains a random mix of both polytypes.

In the Mg−Al LDH system all the interlayer H_2O molecules are removed on heating to 250 °C, thereby causing a decrease in the interlayer spacing from 7.6 to 6.5 Å simultaneously nullifying the geometric factors favoring prismatic interactions. Evidence for the loss of hydrogen bonding is found in the in situ DRIFT measurements (data not shown) which indicated a blue shift in the O−H stretching frequency from 3600 cm^{-1} seen at the ambient temperature to 3690 cm^{-1} at 200−300 °C. Our simulations suggest that, upon dehydration, the $3R_1$ motifs in the LDH transform to the 1H sequence as the latter has a better packing efficiency:

$$\text{AC CB BA AC... } (3R_1) \rightarrow \text{AC AC AC AC... } (1H).$$

This transformation is relatively easy involving a simple translation between successive layers. The CB → AC involves a (a/3, 2b/3) translation while BA → AC involves a (2a/3, b/3) translation. The transformation of the $2H_1$ motifs to 1H

$$\text{AC CA AC... } (2H_1) \rightarrow \text{AC AC AC... } (1H)$$

is relatively more energy intensive as there is no simple translation relationship between the AC and CA layers. The CA → AC transformation involves an internal twist of the [$M(OH)_6$] octahedra. This does not take place, and the $2H_1$ motifs persist in the 1H polytype in the form of turbostratic disorder.

The formation of the 1H polytype in the anhydrous LDH is also driven by the eventual decomposition reaction of the LDH. The latter is a topotactic process resulting in the formation of an oxide with the rock salt structure. Professor Figlarz and co-workers[31] have demonstrated the topotactic relationship between the hexagonal and cubic lattices by electron microscopy. The [001] of the hexagonal lattice is parallel to the [111] of the cubic lattice. Thus, the 1H polytype is an essential precursor to the rock salt oxide phase. In the Zn−Al system, the oxide residue has the wurtzite structure, the formation of which does not require the 1H precursor. Accordingly, the LDH retains the structure of the $3R_1$ polytype, right up to the decomposition temperature. The lower decomposition temperature of the Zn−Al LDH is due to the strong tetrahedral site preference of the Zn^{2+} ion. Consequently, there are no hexagonal hydroxides of Zn. The most stable polymorphic modification of $Zn(OH)_2$ is ϵ-$Zn(OH)_2$, which is isostructural with cubic crystobalite. Brucite-like $Zn(OH)_2$ in which Zn^{2+} ions occupy octahedral sites is a high-pressure phase. All these factors suppress the $3R_1$ → 1H transformation in the Zn−Al system.

Conclusions. In conclusion, we show that the Mg−Al LDH on thermal treatment transforms from the $3R_1$ → 1H polytype facilitating the topotactic decomposition to an oxide having the rock salt structure. Such a transformation is neither energetically feasible nor topochemically necessary in the Zn−Al system where the oxide residue has the wurtzite structure. Whereas the octahedral coordination of Mg^{2+} is preserved in the former case by virtue of this transformation, the coordination of Zn^{2+} changes from octahedral symmetry in the LDH to tetrahedral symmetry in the oxide.

Acknowledgment. The authors thank the Department of Science and Technology (DST), Government of India (GOI), for financial support. G.S.T. thanks the University Grants Commission (UGC), GOI, for the award of a Teacher Fellowship under the FIP program. A.V.R. thanks UGC for the award of a Senior Research Fellowship (NET). S.K. would like to thank DST, New Delhi, for financial assistance sponsored under SERC project scheme (no. SR/S1/PC-35/2003).

References and Notes

(1) Oswald, H. R.; Asper, R. *Preparation and crystal growth of materials with layered structures*; D. Reidel Publishing Company: Dordrecht, The Netherlands; Vol. 1, p 71.
(2) Bookin, A. S.; Drits, V. A. *Clays Clay Miner.* **1993**, *41*, 551.
(3) Cavani, F.; Trifirò, F.; Vaccari, A. *Catal. Today* **1991**, *11*, 173.
(4) Bookin, A. S.; Cherkashin, V. I.; Drits, V. A. *Clays Clay Miner.* **1993**, *41*, 558.
(5) Meyn, M.; Beneke, K.; Lagaly, G. *Inorg. Chem.* **1990**, *29*, 5201.
(6) Vaccari, A. *Appl. Clay Sci.* **1999**, *14*, 161.
(7) Ennadi, A.; Legrouri, A.; De Roy, A.; Besse, J. P. *J. Solid State Chem.* **2000**, *152*, 568.
(8) Kannan, S.; Kishore, D.; Hadjiivanov, K.; Knozinger, H. *Langmuir* **2003**, *19*, 5742.
(9) Constantino, V. R. L.; Pinnavaia, T. J. *Inorg. Chem.* **1995**, *34*, 883.
(10) Rey, F.; Fornes, V.; Rojo, J. M. *J. Chem. Soc., Faraday Trans.* **1992**, *88*, 2233.
(11) Hibino, T.; Tsunashima, A. *J. Mater. Sci. Lett.* **2000**, *19*, 1403.
(12) Rives, V. *Mater. Chem. Phys.* **2002**, *75*, 19.
(13) Taylor, H. F. W. *Miner. Mag.* **1973**, *39*, 377.
(14) Vaysse, C.; Guerlou-Demourgues, L.; Delmas, C. *Inorg. Chem.* **2002**, *41*, 6905.
(15) Millange, F.; Walton, R. I.; O'Hare, D. *J. Mater. Chem.* **2000**, *10*, 1713.
(16) Reichle, W. T. *Solid State Ionics* **1986**, *22*, 135.
(17) Treacy, M. M. J.; Deem, M. W.; Newsam, J. M. *Computer Code DIFFaX, Version 1.807*. NEC Research Institute, Inc.: Princeton, New Jersey, 2000.
(18) Treacy, M. M. J.; Newsam, J. M.; Deem, M. W. *Proc. R. Soc. London* **1991**, *A433*, 499.
(19) Thomas, G. S.; Rajamathi, M.; Kamath, P. V. *Clays Clay Miner.* **2004**, *52*, 693.
(20) Radha, A. V.; Shivakumara, C.; Kamath, P. V. *Clays Clay Miner.* **2005**, *53*, 521.
(21) Zhao, Y.; Li, F.; Zhang, R.; Evans, D. G.; Duan, X. *Chem. Mater.* **2002**, *14*, 4286.
(22) Kloprogge, J. T.; Hickey, L.; Frost, R. L. *J. Solid State Chem.* **2004**, *177*, 4047.
(23) Newman, S. P.; Jones, W.; O'Connor, P.; Stamires, N. *J. Mater. Chem.* **2004**, *12*, 153.

(24) Thomas, G. S.; Kamath, P. V. *J. Chem. Sci. (India)* **2006**, *118*, 127.

(25) Drits, V. A.; Bookin, A. S. *Crystal Structure and X-ray identification of layered double hydroxides*; Nova Science: New York, 2001; p 39−92.

(26) Ramesh, T. N.; Jayashree, R. S.; Kamath, P. V. *Clays Clay Miner*. **2003**, *51*, 570.

(27) Rajamathi, M.; Nataraja, G. D.; Ananthamurthy, S.; Kamath, P. V. *J. Mater. Chem*. **2000**, *10*, 2754.

(28) Bellotto, M.; Rebours, B.; Clause, O.; Lynch, J.; Bazin, D.; Elkaïm, E. *J. Phys. Chem.* **1996**, *100*, 8527.

(29) Sato, T.; Kato**,** K.; Endo, T.; Shimada, M. *React. Solids* **1986**, *2*, 253.

(30) Delahaye-Vidal, A.; Tekaia-Elhsissen, K.; Genin, P.; Figlarz, M. *Eur. J. Solid State Inorg. Chem.* **1994**, *31*, 823.

(31) Figlarz, M.; Gerand, B.; Delahaye-Vidal, A.; Dumont, B.; Harb, F.; Coucou, A.; Fievet, F. *Solid State Ionics* **1990**, *43*, 143.